coatings

Article

Erosion Behavior of Stellite-6 and WC-12Co Coatings on SA213-T22 Boiler Steel

Aumpava Kiatisereekul , Thamrongsin Siripongsakul and Kittichai Fakpan *

Department of Materials and Production Technology Engineering, Faculty of Engineering, King Mongkut's University of Technology North Bangkok, 1518, Pracharat 1 Road, Wongsawang, Bangsue, Bangkok 10800, Thailand
* Correspondence: kittichai.f@eng.kmutnb.ac.th; Tel.: +66-2-5874335

Abstract: At Mae-Moh power plant, Thailand, superheater tubes, which are exposed to a fly ash environment, often degrade due to solid particle erosion. To extend the service lifetime of the superheater tubes, the high velocity oxy-fuel (HVOF) thermal spray technique is used to deposit a protective coating on the material, SA213-T22 steel. In this work, the solid particle erosion of Stellite-6 and WC-12Co coatings was investigated using erodent particle impingement at angles of 30 and 90°. This was carried out with an average particle size of 60 µm. The erosion behavior of SA213-T22 with and without Stellite-6 and WC-12Co coatings was examined using ductile and brittle erosion modes. The erosion testing resulted in the brittle mode for both Stellite-6 and WC-12Co coatings, while the SA213-T22 without coating indicated the ductile mode. On investigation of the surface morphology, the SA213-T22 steel showed ploughing and microcutting. The Stellite-6 coating showed some evidence of ductile erosion such as lips on the coating surface, different from the WC-12Co coating which showed microcracks and deep cavities. The erosion resistance of the Stellite-6 coating was higher than the WC-12Co coating. This was due to the strength and toughness of the metal matrix composite structure and the low porosity of the coating.

Keywords: high velocity oxy-fuel; WC-12Co; Stellite-6; microhardness; erosion; T22 steel

Citation: Kiatisereekul, A.; Siripongsakul, T.; Fakpan, K. Erosion Behavior of Stellite-6 and WC-12Co Coatings on SA213-T22 Boiler Steel. *Coatings* **2023**, *13*, 1444. https://doi.org/10.3390/coatings13081444

Academic Editor: Alexander Modestov

Received: 22 July 2023
Revised: 11 August 2023
Accepted: 13 August 2023
Published: 16 August 2023

1. Introduction

The power industry suffers from severe corrosion and erosion problems, resulting in substantial losses. Erosion results from the impact of particulates, such as coal ash, dolomite and unburned carbon particles on the surface of heated boiler tubes [1]. As a general rule, solid particle erosion refers to the progressive loss of original material due to mechanical interaction between the substrate and the erodent particles carried by the flue gas [2–5]. The solid particle erosion mechanism and erosion rates depend on the particle properties, substrate properties and impingement conditions. Several studies have discussed how particle hardness (H_p) and target hardness (H_t) affect erosion rate [6,7]. Solid particle erosion mechanisms can be divided into two major categories: ductile and brittle. Ductile erosion happens when the material is removed due to cutting and ploughing actions, while brittle erosion is characterized by the formation of cracks and fractures on the material surface [8,9]. The major difference between those two modes can be clarified when erosion rates differ due to different impingement angles. Ductile materials usually show higher erosion rates at shallow impingement angles. On the other hand, erosion rates in the brittle mode are dominant at impingement angles close to the normal angle [10,11]. Recently, thermal spray processes have represented an important and cost effective technique for coating the surface of metals to enhance their durability and performance under a variety of operating conditions. The high velocity oxy-fuel (HVOF) technique is the thermal spray process which forces particles with high kinetic energy to be attached to the surface of the material. The deposited particles are generally in the plastic state, leading to a dense coating [12–14] being obtained. The HVOF spray technique has been found to be a viable coating technique for in situ applications, wear and corrosion management and dimensional restoration, due to its high bonding strength, low porosity and low stress coatings. Kumar et al. reported that the 35 wt% WC + NiCrBSiC coating showed a high level of quality in terms of hardness and low porosity [1,15]. The increase in the WC content from 0 to 35 wt% significantly improved the hardness of the coating without decreasing toughness. Carbide-based coatings have been widely used in abrasive, erosive and oxidizing environments. It was reported that carbide-based coatings exhibited high hardness with a high volume fraction of carbide and high wear resistance [16].

Cobalt has been reported as one of the important elements affecting the hardness and toughness of the materials. Cobalt-alloy coatings are exceptionally good for applications requiring resistance to corrosion, erosion, cavitation and wear. For example, WC-12Co coatings are often used in applications requiring abrasive wear resistance [1,17,18]. When cobalt is added to tungsten carbide, it improves adhesion and wettability [19].

In order to improve the service life of power plant boiler steel SA213-T22, Stellite-6 and WC-12Co coatings were applied to the materials and a comparison of the erosion types was performed. The evaluation of these hard coatings using extremely hard solid particles like silicon carbide (SiC) was never reported. The acceleration test utilized SiC, one of the hardest materials, as an erodent particle in order to clarify the quality of the hard coatings in a short time. Erosion behavior was discussed based on the velocity exponent, the hardness ratio, and the morphology of the target materials.

2. Experimental Section

2.1. Materials and Coating Process

SA213-T22 boiler steel was obtained from the Mae Moh power plant in Lampang province, Thailand. The steel was in a tube shape with a diameter of 50.8 mm and a thickness of 9.1 mm. The chemical composition (wt%) analyzed by a standard emission spectroscopy technique is shown in Table 1.

Table 1. Chemical compositions of SA213-T22 steel [15].

Composition (wt%)	C	Mn	Si	S	P	Cr	Mo	Fe
T22 steel	0.11	0.43	0.27	0.011	0.016	1.93	0.92	Bal.
ASTM SA213-T22	0.15	0.3–0.6	0.5	0.03	0.03	1.9–2.6	0.87–1.13	Bal.

Stellite-6 and WC-12Co powders with particle size of 15–45 µm were used in the HVOF process. The powders and process were supported by the Hummingbird Corporation Co., Ltd., Samut Songkhram, Thailand. The chemical compositions and particle sizes of the coating powders are shown in Table 2. The SA213-T22 steel substrates were prepared with dimensions of 15 mm × 15 mm × 3 mm prior to coating and then they were cleaned with acetone and grit-blasted using an alumina abrasive powder. The coatings were deposited on SA213-T22 steel substrates using an HVOF coating machine, a Termika-3 system. Propane and oxygen were used as fuel and working gases, respectively. The process parameters for the HVOF coating are shown in Table 3. The parameters were optimized by the Hummingbird Corporation Co., Ltd.

Table 2. Composition of HVOF coating powders [20].

Coating Powder	Average Particle Size (µm)	Composition (wt%)				
		C	Si	Cr	Co	W
Stellite-6	11–45 µm, spherical	1	1	28	66	4
WC-12Co	15–45 µm, spherical	4	-	-	12	84

Table 3. Spray parameters employed for HVOF coating.

Parameters	Values
Powder feed rate (g min^{-1})	25
Oxygen flow rate (O_2, L min^{-1})	50
Propane flow rate (C_3H_8, L min^{-1})	20
Air flow rate (L min^{-1})	400
Spray distance (mm)	200
Coating thickness (average, µm)	200
Maximal heat source temperature (°C)	2850

2.2. Erosion Experiments

Silicon carbide (SiC) was used as the erodent material, which is composed of crystalline SiC 98.10 wt%, Si 0.25 wt%, C 0.13 wt%, SiO_2 0.50 wt%, Fe_2O_3 0.12 wt% and other oxides 0.30 wt% by weight. SiC particles have angular, faceted surfaces, and there are no surface defects. Microhardness test results show this erodent to be the hardest at 2481 Hv [21]. According to ASTM G76-05 standard, the accelerated solid particle erosion test was conducted at an ambient temperature using an air-jet type erosion tester as shown in Figure 1 [19]. The erosion tester consists of an air compressor pump, an erodent particle collector, a nozzle with a bore diameter of 6 mm and a sample holder. For each condition, three samples were used to conduct an erosion test and plot a graph using the average data. The results of the report were average erosion rates. In cases where the particle was softer than the target ($H_p/H_t < 1$), the evaluation time was longer and very low erosion rates were observed [21–25]. SiC, one of the hardest materials, was used to clarify erosion rates in a short period of time [26–29]. The diameter of SiC used as an erodent particle is 60 µm. Its morphology is shown in Figure 1.

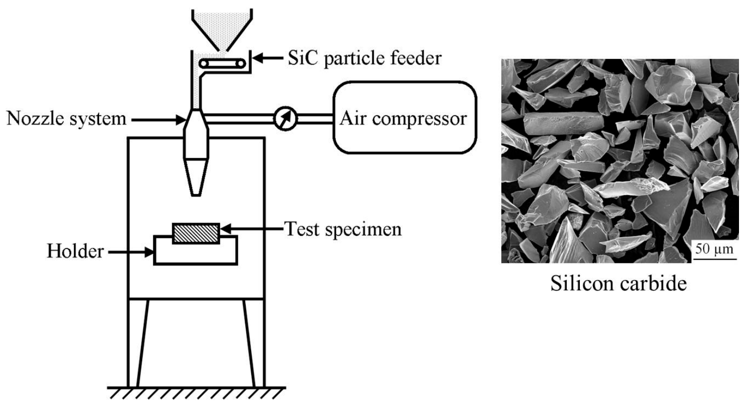

Figure 1. The schematic diagram of the air-jet type erosion tester and SEM micrograph of silicon carbide erodent particles.

The experimental parameters used are shown in Table 4. The average particle size of SiC erodent used in the tests was 60 µm in diameter and the feeding rate was 10 g·min^{-1} with a standoff distance of 20 mm. The erodent particles were accelerated to pass through the nozzle; the particle velocities adjusted by the compressed air with a mass flow controller were 12.8, 22.5 and 38.9 m·s^{-1} for SiC sized 60 µm. The measurement of the particle velocities was carried out using a 1D laser Doppler anemometer (Dantec Dynamics, Skovlunde, Denmark), 1D FlexLDA system. The calibration was supported by National Institute of Metrology, Thailand, and the results will be published elsewhere. It was possible to set the sample holder at the impingement angles of 30 and 90°.

The erosion study was conducted on uncoated SA213-T22 and coated samples with the parameters listed in Table 4. All of the coated samples were first ultrasonically cleaned in alcohol, dried and weighed on an analytical balance (Mettler Toledo, Zurich, Switzerland) having the least count of 0.01 mg precision before testing. Prior to erosion testing, the uncoated samples were mechanically ground using abrasive papers up to 1000 grits, while the coated samples were only cleaned ultrasonically in alcohol for 15 min before being dried. Mass loss was determined after samples were cleaned and dried after exposure to silicon carbide particles. An erosion rate (E) was calculated by dividing the sample mass change (Δm_t) to the particle mass (Δm_p) used in each test cycle with respect to ASTM G76-05. This was carried out according to the following equation [29,30].

$$E = \frac{\Delta m_t}{\Delta m_p} \tag{1}$$

Table 4. Parameters used for erosion testing.

Parameters	Values
Standoff distance (mm)	20
Test gas	Dry air
Test duration (s)	60
Nozzle diameter (mm)	6
Test temperature	Room temperature
Particle velocity (m·s^{-1})	12.8, 22.5 and 38.9
Abrasive feed rate (g min^{-1})	20
Angle of incidence (°)	30, 90
Air jet pressure (bar)	5

Furthermore, volumetric erosion rates were evaluated according to ASTM G76-13. The calculation was based on the following equation [31].

$$E = \frac{\Delta m_t}{D_t \Delta m_p} \tag{2}$$

Here, D_t is the target material density. The SA213-T22 steel, Stellite-6 and WC-12Co densities were 7.80 g/cm^3, 8.46 g/cm^3 and 14.0 g/cm^3, respectively [32–34].

2.3. Characterization

The surface morphology of the samples, both before and after the erosion test was observed using a field emission scanning electron microscope with energy dispersive spectroscopy (EDS) (FE-SEM/EDS) (Tescan, Mira3, Kohoutovice, Czech Republic) to determine the compounds in the coatings. The Vickers test (HV-1000B) was carried out to measure the microhardness of the substrate and coatings. In addition, the surface roughness was evaluated by a 3D laser microscope (Olympus OLS4000-SAF, Olympus, Tokyo, Japan).

3. Results and Discussion

3.1. Characterization

3.1.1. SEM/EDS and X-ray Diffraction Analysis

Figure 2a shows the surface morphology of the HVOF sprayed coating of Stellite-6 as deposited. The coating surface was continuous; a few unmelted particles with diameters ranging from 10 µm to 30 µm were also left. The coating presented a continuous surface but rough texture as a result of unmelted particles. The roughness of the coating was 13.54 µm evaluated by the 3D laser microscope. The cross-sectional micrograph of the coating is shown in Figure 2b. The coating had a small amount of porosity. Using Image J, the image analysis software, the average thickness of the coating was 215 ± 12 µm with an average porosity of 3.29 wt%. A line scanning element analysis in Figure 2c shows that the coating consisted of Co and Cr. Oxygen in the coating was slightly increased compared to the steel substrate.

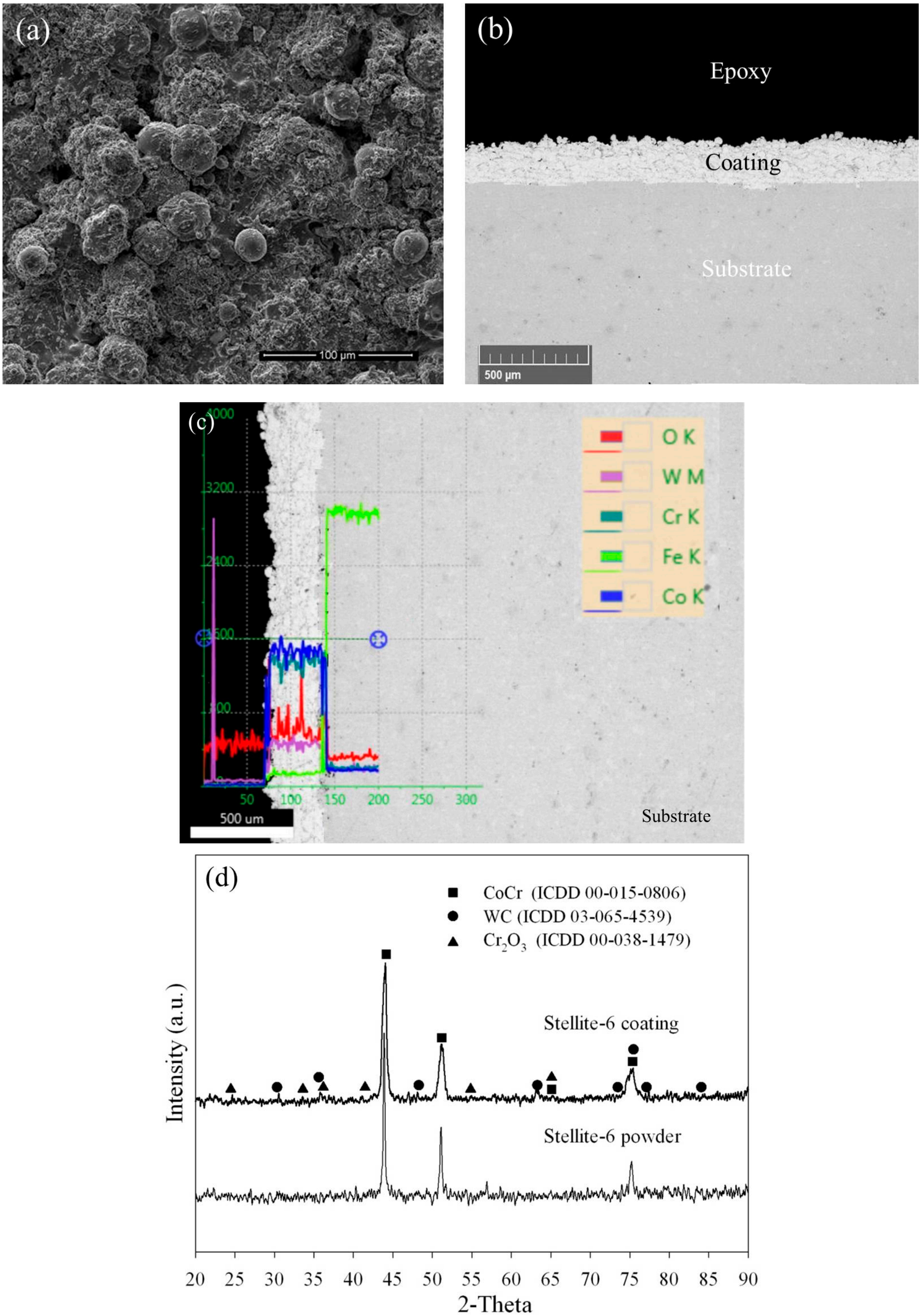

Figure 2. SEM micrographs of (**a**) surface, (**b**) cross-sectional, (**c**) EDS line scan and (**d**) X-ray diffraction patterns of the high velocity oxy-fuel sprayed Stellite-6 coating.

As shown in Figure 2d, the XRD pattern was derived from the top surface of Stellite-6 coating, indicating the composition of CoCr, WC and Cr_2O_3 phases. The Cr_2O_3 phase was not detected from the Stellite-6 powder. According to the line scan and XRD results, oxidation occurred during the high velocity oxy-fuel spray-coating process, forming partially the protective Cr_2O_3 as deposited. The surface morphology of the HVOF sprayed coating of WC-12Co is shown in Figure 3a. A rough surface with small pores and unmelted particles was also observed. The roughness of the coating was 8.85 µm, slightly lower than the Stellite-6 coating. The cross-sectional micrograph of the WC-12Co coating is shown in Figure 3b with the evaluated amount of porosity of 6.73 wt%. The average thickness of the coating was 198 ± 7 µm. The line scanning element analysis of the coating is shown in Figure 3c exhibiting the presence of W, Co Cr and C, while oxide was detected less, compared to the Stellite-6. Stellite-6 had about half the porosity of WC-12Co. This was likely due to the sintering effect of metallic Co and a high binding capability with tungsten carbides in the HVOF coatings [14,19].

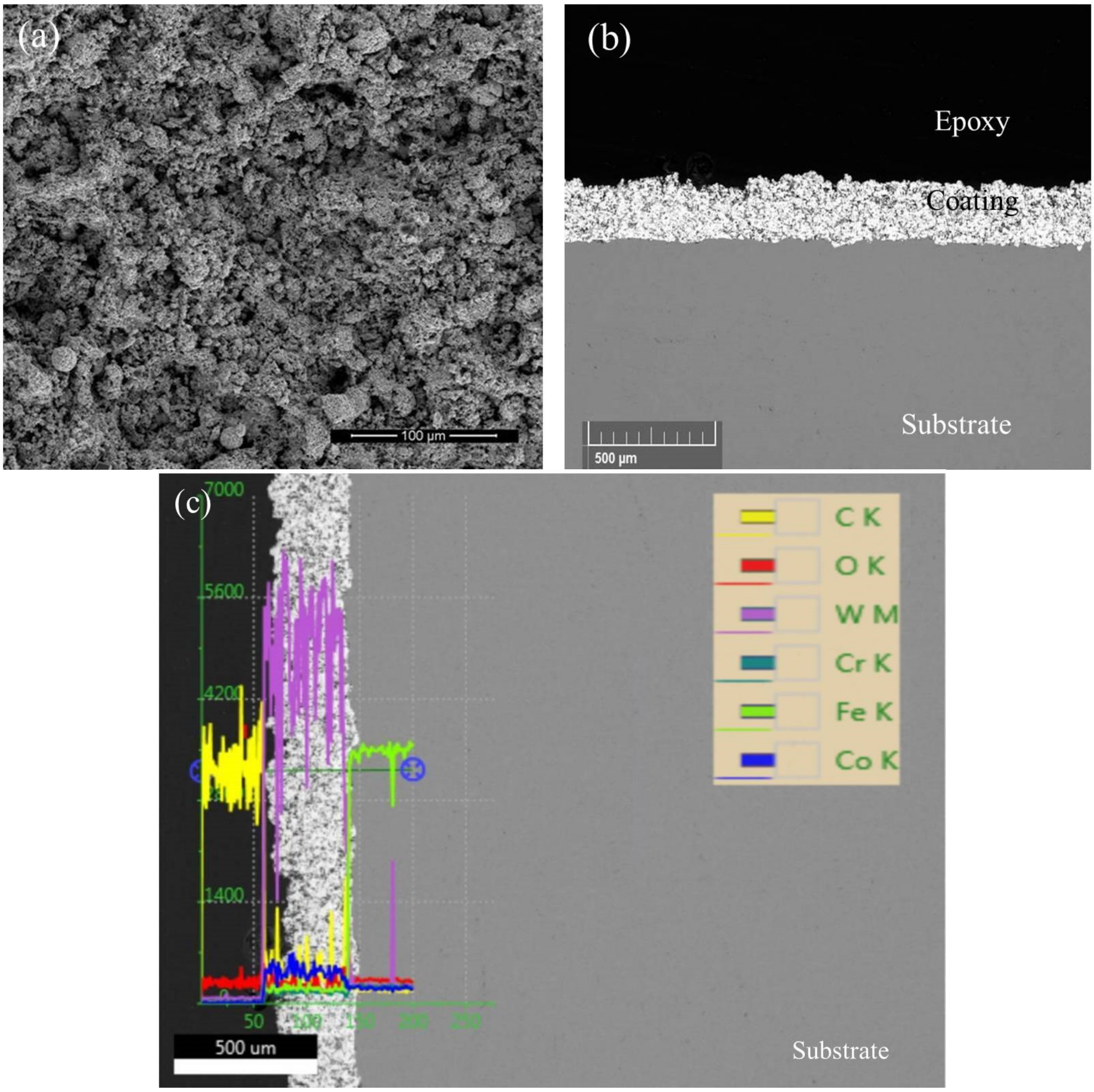

Figure 3. *Cont.*

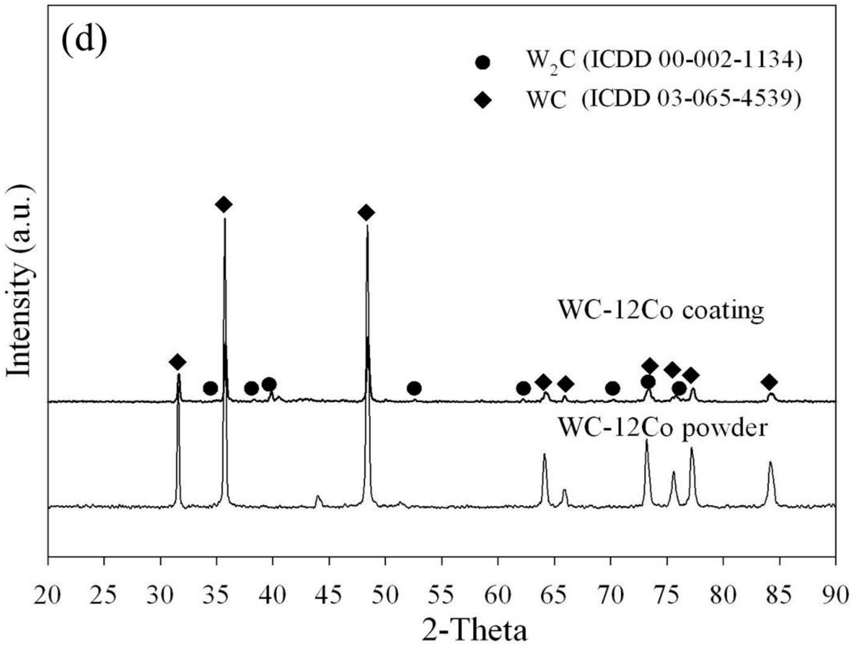

Figure 3. SEM micrographs of (**a**) surface, (**b**) cross-sectional, (**c**) EDS line scan and (**d**) X-ray diffraction patterns of the high velocity oxy-fuel-sprayed WC-12Co coating.

The XRD results of the WC-12Co coating are shown in Figure 3d and indicate the existence of WC and W_2C. The peaks of WC for 2θ values at 31.64, 35.79, 48.45, 64.27, 73.37, 75.72, 77.22, 84.28° are obvious, indicating it as the main phase of the coating. It is well known that in order to achieve an optimum wear property from the WC-M (M=Co, Ni, Cr, Mo) coating, the WC phase should be retained for a large volume fraction [16,35–37], while W_2C and Co were detected with quite low intensity, indicating lower volume fractions of W_2C and metallic Co in the coating. Kreye investigated different phase transformations during HVOF spraying of two different WC-12Co powders [38]. In the cast and crushed types, WC, W_2C, Co_3W_3C and W existed in the coating. A substantial portion of the WC (about 30 to 50 wt%) was transformed to W_2C and W. For the agglomerated and sintered types of WC-12Co powder, only WC and Co were detected. In the HVOF process performed in this study, only a small portion of WC, less than 10 wt%, was transformed to W_2C. The phases of W and Co_3W_3C were not detected in the coating.

3.1.2. Hardness

The microhardness of the SA213-T22 substrate, Stellite-6 and WC-12Co coatings are shown in Figure 4. The average hardness value of the uncoated sample was 143.97 Hv with a discrepancy of 10 Hv, while the coatings produced by the HVOF process yielded values of more than 500 Hv. The average hardness of the WC-12Co coating was 745.67 Hv, while the one of Stellite-6 was 511.12 Hv. The hardness of the Stellite-6 coating was comparable to the one of Stellite-6 coatings reported by Mirsheka [39]. A WC-12Co coating on 316 stainless steel reported by Stack showed a hardness value of 616 Hv that was similar to this result [40]. However, with appropriate parameters and low porosity the hardness of this kind of coatings can reach approximately 1300 (approximately 16 GPa) [21,41,42]. The differences in hardness between the research works could be attributed to the decarburization, carbide grain size and density of the coating which are generated by various conditions in the HVOF process.

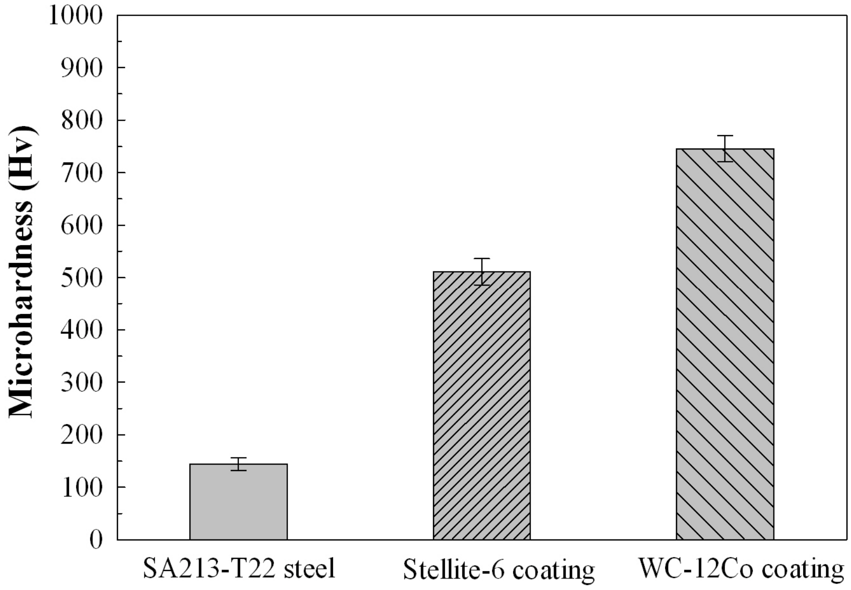

Figure 4. Microhardness of SA213-T22 steel, Stellite-6 and WC-12Co HVOF coatings on SA213-T22 steel substrates.

3.2. Erosion Test

3.2.1. Erosion Rate and Velocity Exponent

Figure 5 shows the steady erosion rates of SA213-T22 steel and the Stellite-6 and WC-12Co coated on SA213-T22 steel tested using silicon carbide as erodent particles with impingement velocities of 12.8, 22.5 and 38.9 m·s^{-1}, and impingement angles of 30 and 90°. All of the erosion rates increased with erodent particle velocity. For Stellite-6 and WC-12Co coatings, the erosion rates at 90° were lower than those at 30°. Especially when the velocity was 12.8 m·s^{-1}, the ratios of erosion rates at 90° to those at 30° (E_{90}/E_{30}) of Stellite-6 and WC-12Co coatings were up to 1.58 and 1.30, respectively. The values of erosion rates as well as E_{90}/E_{30} of all samples are summarized in Table 5. Stellite-6 and WC-12Co coatings exhibited E_{90}/E_{30} values of more than 1, corresponding to erosion in the brittle mode. Conversely, the erosion rates of SA213-T22 steel, uncoated samples, exhibited erosion in the ductile mode with higher erosion rates at 30° than those at 90°; thus the E_{90}/E_{30} values were less than 1. The results relating to impingement angles and erosion modes was in good agreement with the results reported by Roy [43]. According to the erosion test results, the Stellite-6 coating showed better wear resistance than the WC-12Co coating. The inset in Figure 5 shows the volumetric erosion rates of the Stellite-6 and WC-12Co coatings. The Stellite-6 coating wear resistance was not significantly higher than that of the WC-12Co coating. Due to WC-12Co possessing greater hardness than Stellite-6, the wear resistance was supposed to be better, but the volumetric erosion rate was higher as well. This might be caused by the higher porosity of the WC-12Co coating.

Principally, an erosion rate is related to the kinetic energy of erodent particles. The hardness, Young's modulus, mechanical properties, and surface morphology of erodent particles and substrates are also important factors leading to elastic and inelastic collision. Particle velocity is the most influential parameter affecting erosion. Empirically, the erosion rate at room temperature can be expressed by the velocity exponent of the following equation [6,21,24,29,30,44,45]:

$$E = Kv^n \tag{3}$$

where E is the erosion or wastage rate, v is the impingement velocity, K is a material constant and n is a velocity exponent dependent on the material of the erodent particles and substrates. The erosion rates were fitted well using Equation (3), as shown in Figure 5, by solid lines (90° impingement angle) and dotted lines (30° impingement angle) with the correlation coefficients of more than 0.91. The value of the velocity exponent is another parameter used to determine the ductile or brittle erosion. Such as for SA213-T22 steel which showed ductile erosion behavior, the velocity exponent changed widely from 2.31 at 30° to 3.23 at 90° impingement angles. This drastic change indicated the sensitivity to erosion of the surface condition of the material [7]. The value at 30° was under Basu, who suggested that the velocity exponent value was 2.3–2.7 for ductile materials, while SiC embedment at 90° impingement caused the SA213-T22 surface to become a composite or brittle material; therefore, the velocity exponent could exceed 3 [3,46]. For ductile erosion, erosion rates were higher at a 30° than at a 90° impingement angle. A surplus amount of energy was required at the 90° impingement angle for target deformation [21,30,43,47].

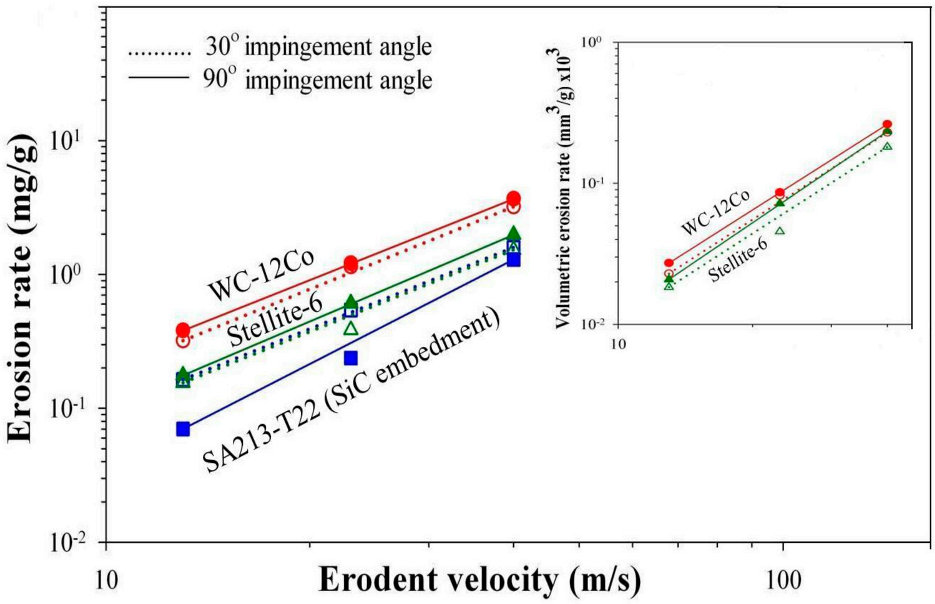

Figure 5. Erosion rates of SA213-T22 steel (blue line), Stellite-6 (green line) and WC-12Co (red line) HVOF coatings tested by various impingement velocities of erodent particles, and volumetric erosion rates (in the inset) at impingement angles of 30° (dotted markers) and 90° (solid markers).

Table 5. Erosion rates, erosion ratio and velocity exponent of uncoated samples, Stellite-6 and WC-12Co coated samples.

Sample	Impingement Angle (°)	Erodent Particle Velocity (m/s)	Erosion Rate (mg/g)	Velocity Exponent (*n*)	E_{90}/E_{30}	Comment
SA213-T22	30	12.8	0.16 ± 0.02			
		22.5	0.54 ± 0.01	2.04		
		38.9	1.59 ± 0.13			
	90	12.8	0.07 ± 0.01		0.43	ductile
		22.5	0.24 ± 0.02	2.62	0.44	ductile
		38.9	1.29 ± 0.13		0.81	ductile
Stellite-6	30	12.8	0.16 ± 0.01			
		22.5	0.38 ± 0.01	2.06		
		38.9	1.53 ± 0.18			
	90	12.8	0.18 ± 0.02		1.14	brittle
		22.5	0.61 ± 0.04	2.15	1.58	brittle
		38.9	1.98 ± 0.11		1.29	brittle
WC-12Co	30	12.8	0.32 ± 0.07			
		22.5	1.14 ± 0.12	2.07		
		38.9	3.20 ± 0.31			
	90	12.8	0.38 ± 0.07		1.19	brittle
		22.5	1.21 ± 0.08	2.04	1.06	brittle
		38.9	3.66 ± 0.19		1.14	brittle

Thus, the higher velocity exponent responded to lower erosion rates than those at 30°. The values of the velocity exponent are also summarized in Table 5. The velocity exponents of Stellite-6 and WC-12Co coatings were approximately 2; this followed the traditional rules using SiC as an erodent particle, as reported in other literature [3,28,46].

When the erodent particle velocity was 38.9 m/s, the erosion rates of uncoated SA213-T22 substrates were 0.2–0.3 mg/g, and those of samples with Stellite-6 and WC-12Co coatings were approximately 0.4 and 2.0 mg/g, respectively. The results of the uncoated samples were comparable to the erosion rates of steels as reported by Sapate, when alumina was used as the erodent particle [47]. In comparison to Singh's report, this work had approximately one-order higher erosion rates than WC-12Co and Stellite-6 coated samples tested using alumina erodent [14]. SiC erodent particles have a greater hardness of 2481 Hv than alumina particles, resulting in the difference [21]. In addition to the above factors, the porosity, density, and chemical composition of the coated samples also played a role in the erosion behavior.

3.2.2. Surface Morphology and Chemical Composition Analysis

To understand the erosion behavior, the surface of the sample after the erosion test was investigated using FE-SEM with EDX. The SEM micrographs with the EDX analysis results of the uncoated SA213-T22 steel, the Stellite-6- and WC-12Co-coated samples after the erosion tests at 30 and 90° impingement angles are shown in Figures 6–8.

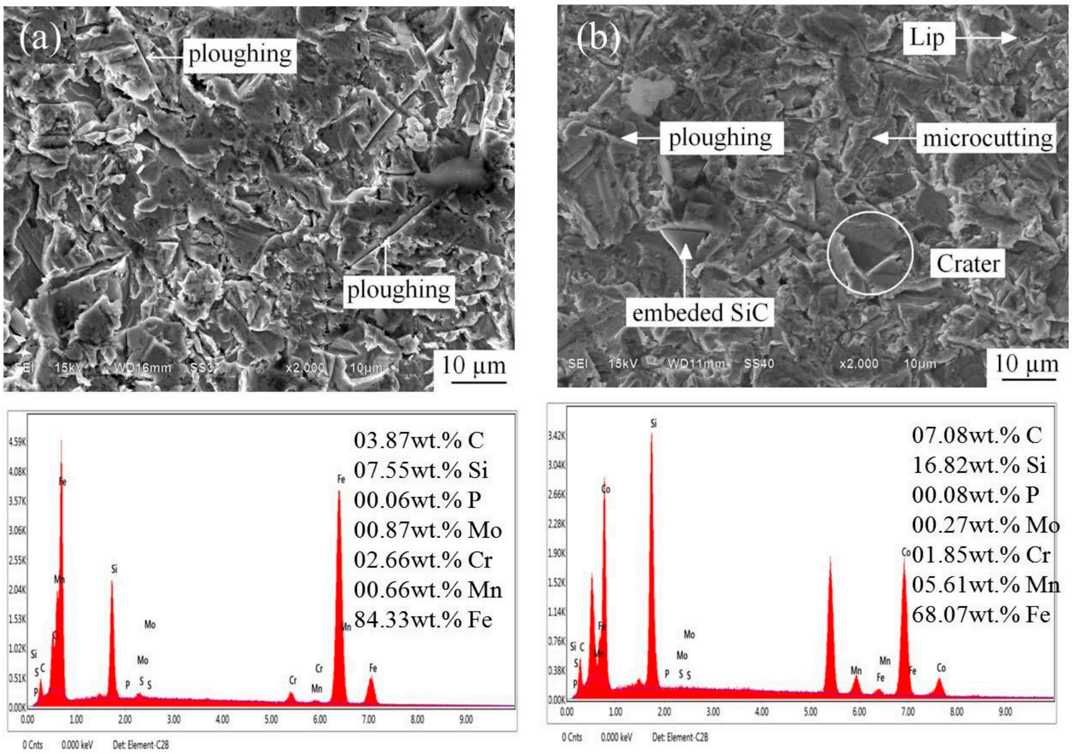

Figure 6. SEM images (upper) and EDX (lower) analysis results of SA213-T22 steel after the erosion test at velocity of 22.5 m/s at impingement angle (**a**) 30° (**b**) 90°.

The EDX analysis of the eroded SA213-T22 surface at 30 and 90° impingement angles is shown in Figure 6a,b. The detected chemical composition of Fe, Cr, Mo, C, Mn, S, P and Si was in conformance with SA213-T22 steel. The presence of Si along with C clearly indicated that the erodent (SiC) had incrusted the substrate, as the Si to C ratios by mole after the erosion tests at 30 and 90° impingement angles were 1:1.12 and 1:0.98, respectively. The same result was reported for SiC embedding [1]. Thus, the embedment of SiC on the steel surface was misleading by giving low erosion rates in the aforementioned results. However, the velocity exponent was quite sensitive to this phenomenon, and showed high sensitivity to erosion of SA213-T22. The inclusion of SiC mass after the erosion tests at 90° was twice that at 30°. This was also the reason for the low erosion rate at the normal angle of ductile materials.

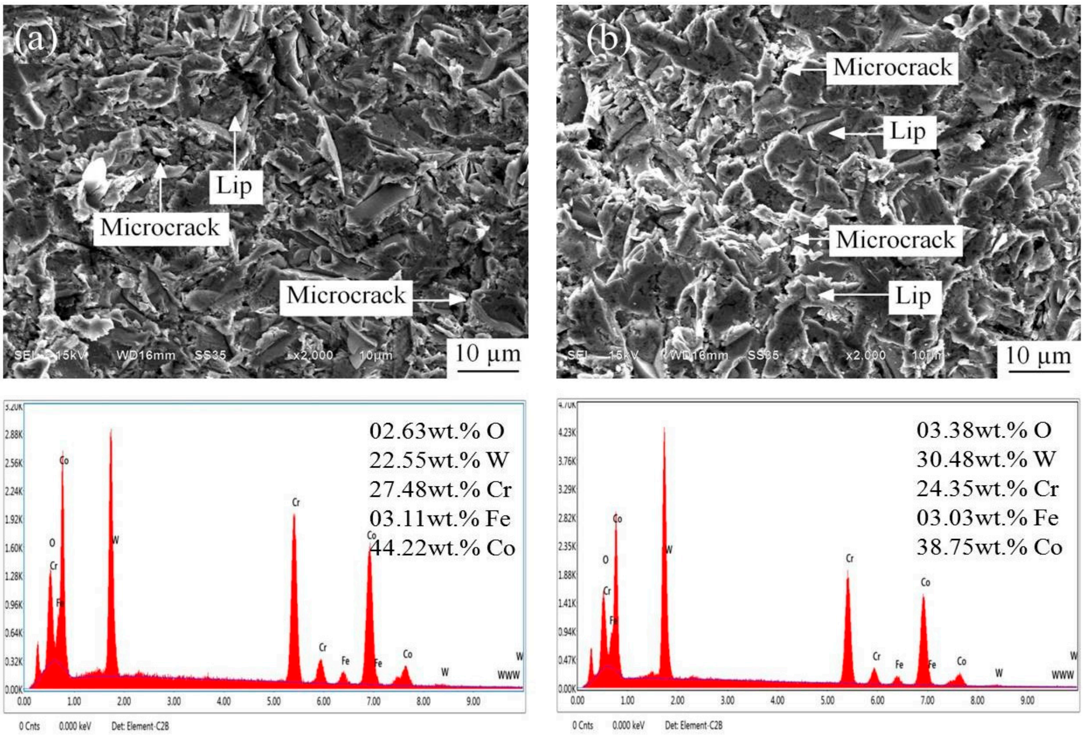

Figure 7. SEM/EDAX image of Stellite-6 at velocity of 22.5 m/s at impingement angle (**a**) 30° (**b**) 90°.

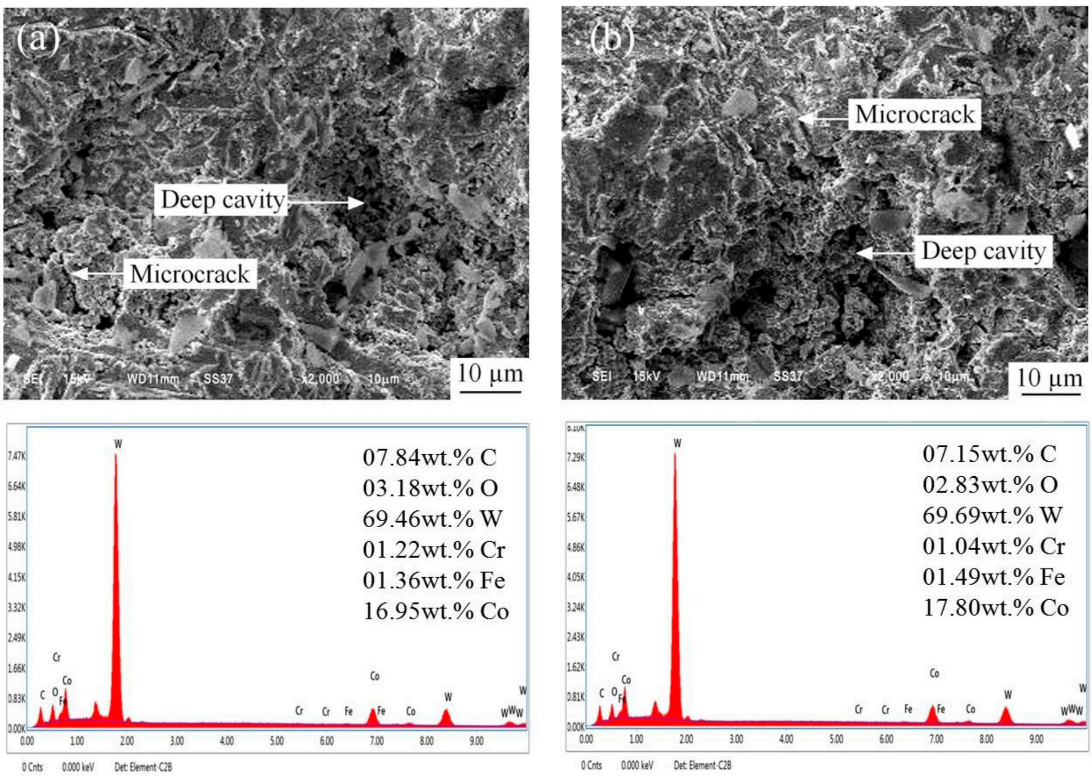

Figure 8. SEM/EDAX image of WC-12Co at velocity of 22.5 m/s at impingement angle (**a**) 30° (**b**) 90°.

The surfaces of the Stellite-6 coating tested under impingement angles of 30 and 90° are shown in Figure 7a,b, respectively. The composition indicated Co, Cr, W, Fe and a small amount of oxide. On the other hand, W, C, Co, Cr, Fe and O were detected in WC-12Co coatings, as shown in Figure 8a,b. According to both EDX results, there was no detection of Si; thus, SiC embedment did not occur on samples with Stellite-6 and WC-12Co coatings.

In general, the erosion characteristics of ductile materials at shallow impingement angles are dominated by ploughing, crater, cutting and shear deformation. Meanwhile at the normal impingement angle, low cycle fatigue and localization of plastic flow can occur. As is well known, erosion mechanisms are controlled by the ratio of erodent particle hardness (H_p) to target hardness (H_t). The ratio of erodent particle hardness to target surface hardness (H_p/H_t) has to be considered for evaluating coating-erosion behavior. Experimental results indicated that abrasive particles would cause plastic scratching and indent the surface only if H_p/H_t was more than 1.2 [1,6,48]. In cases where the particle was softer than the target (H_p/H_t is less than 1), very low erosion rates were observed [25]. In the case of SA213-T22 steel, the H_p/H_t ratio of 17.23 indicated ductile erosion with plastic deformation resulting in SiC particle penetration into the substrate surface. The SEM image in Figure 6a shows the morphology after the erosion test at 30°. Tracks of ploughing lines can be clearly found. The surface after the 90° test in Figure 6b shows microcutting, and embedded SiC. Sequentially, shielding affects against erodent particles due to embedment of hard SiC can lead to apparently low erosion rates. The impingement at an angle at 30° results in more ploughing lines but less SiC embedment.

On the impingement surface of Stellite-6 and WC-12Co coatings, the erosion behavior played a role in crack nucleation and propagation. Figure 7a,b show microcracks and lips within the Stellite-6 coating. In spite of the fact that the E_{90}/E_{30} ratio was greater than 1, ductile erosion was also observed on the Stellite-6 coating. As the H_p/H_t ratio of Stellite-6 coating was 4.85 Hv, this indicated that plastic deformation such as LIBS was possible to detect when much harder erodent particles were used in the test. In addition, Stellite-6 should exhibit metal ductility and toughness rather than brittleness since it is a metal matrix composite. In contrast, Figure 8a,b show microcracks and deep cavities showing de-bonding due only to brittle erosion on the WC-12Co coating. Deep cavities were clearer on the eroded surface tested at the impingement angle at 90° in Figure 8b than those found at 30° in Figure 8a. The H_p/H_t ratio of WC-12Co coating was 3.33 Hv, the lowest of all samples with the E_{90}/E_{30} ratio exceeding 1, which indicated brittle erosion. The brittle behavior was also caused by the cermet composite material itself. Porosity was another factor that affected the morphology after erosion testing as well as the H_p/H_t ratio of WC-12Co coating. This resulted in high erosion rates despite having a higher hardness than the Stellite-6 coatings. The improvement in the erosion resistance of the Stellite-6 coating was also contributed to by the increase in strength and toughness due to the added cobalt content [19]. Further, the compatibility with the HVOF process resulted in the coating's high hardness and low porosity. The erosion of coatings is more complex than that of pure materials. It should be said that hardness is the principal factor affecting erosion. In a situation with various solid particles, pure materials will always suffer from an erosion attack more than those with coatings of hard materials. However, the morphology, such as the porosity of the coating, is also another factor. XRD results showed Stellite-6 coating to be a composite material with WC as its hard phase and CoCr as its matrix. With such a phase composition, a high quality coating with low porosity can be produced using the HVOF process. In contrast, the WC-12Co coating, which had WC with W_2C brittle phases, had a high potential to be optimized to achieve even better coatings due to the higher hardness of the coatings.

4. Conclusions

The HVOF process was used to deposit Stellite-6 and WC-12Co coatings on boiler tube steel, SA213-T22. This resulted in a moderately high hardness, low porosity and a dense coating. Erosion testing was carried out for uncoated and coated samples using SiC to clarify the erosion rates in a short period of time. The conclusions can be drawn as follows.

1. The erosion of uncoated SA213-T22 steel showed a ductile mode with a ploughing and microcutting morphology and SiC embedment on the surface. The erosion rates were lower than the intrinsic values due to the change in the surface condition from metal to composite. Thus, an evaluation of the erosion for materials with extremely low hardness, less than SiC, will result in errors. In the case of high hardness materials such as Stellite-6 and WC-12Co, SiC embedment did not occur on the surface. This made it possible to apply SiC as an erodent particle for erosion testing.
2. The velocity exponent indicates erosion sensitivity. In the case of uncoated SA213-T22 steel with SiC embedment, the change in velocity exponent from 2.3 to a value exceeding 3 showed a drastic change in the surface condition, while the Stellite-6 and WC-12Co coatings had values of 2, which corresponded to the traditional literature [3,27,42].
3. Stellite-6 is a metal matrix composite, whereas WC-12Co coating is a cermet composite. As a result, erosion will behave differently. In the case of a cermet composite, WC-12Co coating showed only brittle erosion, while Stellite-6 showed a morphology with some evidence of ductile erosion such as lips on the coating surface. Thus, its erosion behavior exhibited predominantly brittle erosion.
4. The evaluation results showed better wear resistance from the Stellite-6 than from the WC-12Co coating. This contributed to the strength and toughness of the metal matrix composite structure and the lower porosity of the coating. In the case of the WC-12Co coating, the porosity was double that of the Stellite-6 coating. However, due to the higher hardness of WC-12Co, it has high potential to be optimized to achieve even better coatings if it could reduce its porosity and W_2C brittle phase.

Author Contributions: Conceptualization, A.K. and K.F.; methodology, A.K. and K.F.; validation, T.S.; formal analysis, T.S.; investigation, A.K. and K.F.; resources, A.K. and K.F.; data curation, A.K. and T.S.; writing—original draft preparation, A.K.; writing—review and editing, T.S. and K.F.; visualization, A.K. and K.F.; supervision, K.F.; project administration, T.S. and K.F.; funding acquisition, T.S. All authors have read and agreed to the published version of the manuscript.

Funding: This research was funded by King Mongkut's University of Technology North Bangkok, Thailand (KMUTNB-FF-65-31).

Institutional Review Board Statement: Not applicable.

Informed Consent Statement: Not applicable.

Data Availability Statement: All data that support the findings of this study are included within the article.

Acknowledgments: The authors acknowledge the kind support for materials (SA213–T22 boiler steel) provided by Maemoh Power Plant, Electricity Generating Authority of Thailand (EGAT) and the high velocity oxy-fuel spraying system supported by Hummingbird Corporation Co., Ltd.

Conflicts of Interest: The authors declare no conflict of interest.

References

1. Ramesh, M.; Prakash, S.; Nath, S.; Sapra, P.K.; Venkataraman, B. Solid particle erosion of HVOF sprayed WC-Co/NiCrFeSiB coatings. *Wear* **2010**, *269*, 197–205. [CrossRef]
2. Sundararajan, G. The solid particle erosion of metallic materials: The rationalization of the influence of material variables. *Wear* **1995**, *186*, 129–144. [CrossRef]
3. Sundararajan, G.; Roy, M. Solid particle erosion behaviour of metallic materials at room and elevated temperatures. *Tribol. Int.* **1997**, *30*, 339–359. [CrossRef]
4. Chawla, V.; Chawla, A.; Puri, D.; Prakash, S.; Gurbuxani, P.G.; Sidhu, B.S. Hot corrosion & erosion problems in coal based power plants in India and possible solutions–a review. *J. Met. Mater. Miner.* **2011**, *10*, 367.
5. Levy, A. Erosion and erosion-corrosion of metals. *Corrosion* **1995**, *51*, 872–883. [CrossRef]
6. Shipway, P.; Hutchings, I. The role of particle properties in the erosion of brittle materials. *Wear* **1996**, *193*, 105–113. [CrossRef]

7. Wichianrat, P.; Dateraksa, K.; Sujirote, K.; Chumphu, A. Wear behaviour of alumina nozzles by sand blasting. *J. Met. Mater. Miner.* **2010**, *20*, 15–18.
8. Vite-Torres, M.; Laguna-Camacho, J.R.; Baldenebro-Castillo, R.E.; Gallardo-Hernández, E.A.; Vera-Cárdenas, E.E.; Vite-Torres, J. Study of solid particle erosion on AISI 420 stainless steel using angular silicon carbide and steel round grit particles. *Wear* **2013**, *301*, 383–389. [CrossRef]
9. Ball, A. The mechanisms of wear, and the performance of engineering materials. *J. S. Afr. Inst. Min. Metall.* **1986**, *86*, 1–13.
10. Wellman, R.; Nicholls, J. High temperature erosion–oxidation mechanisms, maps and models. *Wear* **2004**, *256*, 907–917. [CrossRef]
11. Bonu, V.; Barshilia, H.C. High-Temperature Solid Particle Erosion of Aerospace Components: Its Mitigation Using Advanced Nanostructured Coating Technologies. *Coatings* **2022**, *12*, 1979. [CrossRef]
12. Mangla, A.; Chawla, V.; Singh, G. Comparative study of hot corrosion behavior of HVOF and plasma sprayed Ni20Cr coating on SA213 (T22) boiler steel in Na_2SO_4-60% V_2O_5 environment. *Int. J. Eng. Sci. Res. Technol.* **2017**, *4*, 2348–8034.
13. Sapate, S.; Roy, M. Solid particle erosion of thermal sprayed coatings. In *Thermal Sprayed Coatings and Their Tribological Performances*; IGI Global: Hershey, PA, USA, 2015; pp. 193–226.
14. Singh, P.K.; Mishra, S. Erosion performance of detonation gun deposited WC–12Co, Stellite 6 and Stellite 21 coatings on SAE213-T12 steel. *Tribol.-Mater. Surf. Interfaces* **2020**, *14*, 229–239. [CrossRef]
15. Kumar, M.; Singh, H.; Singh, N.; Joshi, R.S. Erosion–corrosion behavior of cold-spray nanostructured Ni–20Cr coatings in actual boiler environment. *Wear* **2015**, *332*, 1035–1043. [CrossRef]
16. Sidhu, H.S.; Sidhu, B.S.; Prakash, S. Mechanical and microstructural properties of HVOF sprayed WC–Co and Cr_3C_2–NiCr coatings on the boiler tube steels using LPG as the fuel gas. *J. Mater. Process. Technol.* **2006**, *171*, 77–82. [CrossRef]
17. Kim, H.J.; Hwang, S.Y.; Lee, C.H.; Juvanon, P. Assessment of wear performance of flame sprayed and fused Ni-based coatings. *Surf. Coat. Technol.* **2003**, *172*, 262–269. [CrossRef]
18. Sharma, A.; Goel, S. Erosion behaviour of WC–10Co–4Cr coating on 23-8-N nitronic steel by HVOF thermal spraying. *Appl. Surf. Sci.* **2016**, *370*, 418–426.
19. Sierens, A.; Vanvooren, J.; Deplus, K.; Faes, K.; De Waele, W. Review on the possible tool materials for friction stir welding of steel plates. In *Sustainable Construction and Design*; Laboratory Soete, Ghent University: Ghent, Belgium, 2014; Volume 5.
20. Peat, T.; Galloway, A.; Toumpis, A.; McNutt, P.; Iqbal, N. The erosion performance of particle reinforced metal matrix composite coatings produced by co-deposition cold gas dynamic spraying. *Appl. Surf. Sci.* **2017**, *396*, 1623–1634. [CrossRef]
21. Suckling, M.; Allen, C. Critical variables in high temperature erosive wear. *Wear* **1997**, *203*, 528–536. [CrossRef]
22. Hejwowski, T.; Szala, M. Wear-Fatigue Study of Carbon Steels. *Adv. Sci. Technol. Res. J.* **2021**, *15*, 179–190. [CrossRef]
23. Weronski, A.; Hejwowski, T. Effect of stress on abrasive and erosive wear of steels and sprayed coatings. *Vacuum* **2008**, *83*, 229–233. [CrossRef]
24. *ASTM G76-05*; Standard Practice for Conducting Erosion Tests by Solid Particle Impingement Using Gas Jets. ASTM International West Conshohocken: Conshohocken, PA, USA, 1983.
25. Heath, G.; Stack, M.; Rehberg, M.; Kammer, P. *The Erosion of Functionally Graded Coatings under Fluidized Bed Conditions*; Presses Polytechniques et Universitaires Romandes: Lausanne, Switzerland, 1995.
26. Promdirek, P.; Chandra-Ambhom, S.; Prasong, R.; Riittirat, S.; Pompaisansakul, N. Influence of gas tungsten arc welding parameters on the high-temperature erosion-corrosion resistance of Incoloy 800 cladded by Stellite 12 for the application as thermowell. *Mater. Sci. Forum* **2011**, *696*, 248–253. [CrossRef]
27. Promdirek, P.; Chandra-Ambhom, S.; Tongtae, C.; Anantawirun, C.; Buaphuen, C. Characterization and Failure Analysis of Incoloy 800 Used as Thermowell Subjected to High Temperature Erosion-Corrosion. *Mater. Sci. Forum* **2008**, *595–598*, 673–680. [CrossRef]
28. Finnie, I. Erosion of surfaces by solid particles. *Wear* **1960**, *3*, 87–103. [CrossRef]
29. Liu, Z.; Wan, S.; Nguyen, V.; Zhang, Y. A numerical study on the effect of particle shape on the erosion of ductile materials. *Wear* **2014**, *313*, 135–142. [CrossRef]
30. Tabakoff, W.; Shanov, V. Erosion rate testing at high temperature for turbomachinery use. *Surf. Coat. Technol.* **1995**, *76*, 75–80. [CrossRef]
31. *ASTM G76-13*; Standard Test Method for Conducting Erosion Tests by Solid Particle Impingement Using Gas Jets. ASTM International West Conshohocken: Conshohocken, PA, USA, 2018.
32. *ASTM A213 T22*; 2.25Cr-1Mo Steel for Boiler and Heat Exchanger Seamless Tubes (STBA 24). ASTM International West Conshohocken: Conshohocken, PA, USA, 2023. Available online: https://www.matweb.com (accessed on 11 August 2023).
33. Cinca, N.; Lopez, E.; Dosta, S.; Guilemany, J. Study of stellite-6 deposition by cold gas spraying. *Surf. Coat. Technol.* **2013**, *232*, 891–898. [CrossRef]
34. Ma, N.; Guo, L.; Cheng, Z.; Wu, H.; Ye, F.; Zhang, K. Improvement on mechanical properties and wear resistance of HVOF sprayed WC-12Co coatings by optimizing feedstock structure. *Appl. Surf. Sci.* **2014**, *320*, 364–371. [CrossRef]
35. Berget, J. Influence of Powder and Spray Parameters on Erosion and Corrosion Properties of HVOF Sprayed WC-Co-Cr Coatings. Ph.D. Thesis, Department of Machine Design and Materials Technology, Norwegian University of Science and Technology, Trondheim, Norway, 1998.
36. Yuan, J.; Zhan, Q.; Huang, J.; Ding, S.; Li, H. Decarburization mechanisms of WC–Co during thermal spraying: Insights from controlled carbon loss and microstructure characterization. *Mater. Chem. Phys.* **2013**, *142*, 165–171. [CrossRef]

37. Ding, X.; Ke, D.; Yuan, C.; Ding, Z.; Cheng, X. Microstructure and cavitation erosion resistance of HVOF deposited WC-Co coatings with different sized WC. *Coatings* **2018**, *8*, 307. [CrossRef]
38. Kreye, H. Characteristics of coatings produced by high velocity flame spraying. *Therm. Spray.* **1989**, *2*, 24.
39. Mirshekari, G.; Daee, S.; Bonabi, S.F.; Tavakoli, M.; Shafyei, A.; Safaei, M. Effect of interlayers on the microstructure and wear resistance of Stellite 6 coatings deposited on AISI 420 stainless steel by GTAW technique. *Surf. Interfaces* **2017**, *9*, 79–92. [CrossRef]
40. Stack, M.; Mathew, M. Transitions in microabrasion mechanisms for WC-Co (HVOF) coated steel, Proceedings of the Institution of Mechanical Engineers. *Part J J. Eng. Tribol.* **2005**, *219*, 49–57. [CrossRef]
41. Jonda, E.; Szala, M.; Sroka, M.; Łatka, L.; Walczak, M. Investigations of cavitation erosion and wear resistance of cermet coatings manufactured by HVOF spraying. *Appl. Surf. Sci.* **2023**, *608*, 155071. [CrossRef]
42. Jonda, E.; Latka, L. Comparative analysis of mechanical properties of WC-based cermet Coatings sprayed by HVOF onto AZ31 magnesium alloy substrates. *Adv. Sci. Technol. Res. J.* **2021**, *15*, 57–64. [CrossRef]
43. Roy, M.; Ray, K.; Sundararajan, G. An analysis of the transition from metal erosion to oxide erosion. *Wear* **1998**, *217*, 312–320. [CrossRef]
44. Kumar, K.; Kumar, S.; Singh, G.; Singh, J.P.; Singh, J. Erosion wear investigation of HVOF sprayed WC-10Co4Cr coating on slurry pipeline materials. *Coatings* **2017**, *7*, 54. [CrossRef]
45. Arabnejad, H.; Mansouri, A.; Shirazi, S.; McLaury, B. Evaluation of solid particle erosion equations and models for oil and gas industry applications. In Proceedings of the SPE Annual Technical Conference and Exhibition, Houston, TX, USA, 27–30 September 2015.
46. Basu, P.; Kefa, C.; Jestin, L. *Boilers and Burners: Design and Theory*; Springer Science & Business Media: Berlin/Heidelberg, Germany, 2012.
47. Sapate, S.; RamaRao, A. Effect of erodent particle hardness on velocity exponent in erosion of steels and cast irons. *Mater. Manuf. Process.* **2003**, *18*, 783–802. [CrossRef]
48. Keshavamurthy, R.; Naveena, B.; Sekhar, N. Thermal spray coatings for erosion-corrosion protection. In *Production, Properties, and Applications of High Temperature Coatings*; IGI Global: Hershey, PA, USA, 2018; pp. 246–267.